Interface focus

J. R. Soc. Interface (2010) **7**, S615–S629
doi:10.1098/rsif.2010.0127.focus
Published online 26 May 2010

Customized Ca–P/PHBV nanocomposite scaffolds for bone tissue engineering: design, fabrication, surface modification and sustained release of growth factor

Bin Duan and Min Wang*

Department of Mechanical Engineering, The University of Hong Kong, Pokfulam Road, Hong Kong

Integrating an advanced manufacturing technique, nanocomposite material and controlled delivery of growth factor to form multifunctional tissue engineering scaffolds was investigated in this study. Based on calcium phosphate (Ca–P)/poly(hydroxybutyrate-co-hydroxyvalerate) (PHBV) nanocomposite microspheres, three-dimensional Ca–P/PHBV nanocomposite scaffolds with customized architecture, controlled porosity and totally interconnected porous structure were successfully fabricated using selective laser sintering (SLS), one of the rapid prototyping technologies. The cytocompatibility of sintered Ca–P/PHBV nanocomposite scaffolds, as well as PHBV polymer scaffolds, was studied. For surface modification of nanocomposite scaffolds, gelatin was firstly physically entrapped onto the scaffold surface and heparin was subsequently immobilized on entrapped gelatin. The surface-modification improved the wettability of scaffolds and provided specific binding site between conjugated heparin and the growth factor recombinant human bone morphogenetic protein-2 (rhBMP-2). The surface-modified Ca–P/PHBV nanocomposite scaffolds loaded with rhBMP-2 significantly enhanced the alkaline phosphatase activity and osteogenic differentiation markers in gene expression of C3H10T1/2 mesenchymal stem cells. Together with osteoconductive nanocomposite material and controlled growth factor delivery strategies, the use of SLS technique to form complex scaffolds will provide a promising route towards individualized bone tissue regeneration.

Keywords: nanocomposite; scaffold; selective laser sintering; surface modification; bone tissue engineering

1. INTRODUCTION

Combining living cells with biodegradable materials and/or bioactive component(s), the concept of tissue engineering first elucidated in the early 1990s represented a paradigm shift from tissue grafting, with autograft being considered as golden standard, or even completely from prosthesis implantation (Langer & Vacanti 1993; Hollister 2009*a*). Currently, several strategies are investigated by many researchers to maintain, repair or improve various tissue functions. For cell-based tissue engineering, autologous or allogeneic cells, either determined or capable of differentiation, are first isolated. The obtained cells with or without target gene transfection are then injected in single cell suspensions or can be further manipulated by cellular assembly into multi-cellular spheroid or cell sheet for transplantation (Matsuda *et al.* 2007; Lin & Chang 2008; Mason & Dunnill 2009). Another strategy is based on the biodegradable scaffold or matrix. Cells and/or biomolecules are encapsulated within the matrices or seeded onto the surface of three-dimensional scaffolds. The matrices or scaffolds serve as extracellular matrix to direct cell adhesion, proliferation and differentiation, and thus promote tissue regeneration. Currently, acellular scaffolds with or without biomolecules such as growth factors, cytokines and peptides are considered as an effective strategy for certain tissue repair because of their smaller costs and easier access to gain surgeon acceptance and regulatory approval (Lysaght *et al.* 2008).

For scaffold-based tissue engineering, although ideal scaffolds have not been achieved yet (or actually there are no such ideal models and each design should follow specific tissue requirements), certain minimum criteria should be met, *viz.*, biocompatibility, mechanical properties similar to the target tissue,

*Author for correspondence (memwang@hku.hk).

One contribution to a Theme Supplement 'Scaling the heights—challenges in medical materials: an issue in honour of William Bonfield, Part II. Bone and Tissue Engineering'.

Received 4 March 2010
Accepted 6 May 2010

biodegradability at a rate commensurate with tissue formation rate, etc. Importantly, multiple pore size distribution, interconnected pore structure and high porosity of scaffolds will facilitate vascularization and diffusion of nutrients and gases. They will also affect the mechanical properties and degradation rate of the scaffolds. Generally, according to the capacity of scaffold architecture control, there are two categories of technologies for scaffold manufacture: the non-designed manufacturing techniques and designed manufacturing techniques (Hollister 2009*b*). Non-designed manufacturing techniques include most of the traditional scaffold fabrication methods, such as solvent casting/particulate leaching, phase separation, melt moulding and electrospinning. Some of these methods can partially control the scaffold architecture by altering certain processing parameters, e.g. porogen size, freezing temperature, applied organic solvents or electrospun fibre collection method (Sundaray *et al.* 2004; Cao *et al.* 2006; Hollister 2009*b*; Liu & Ma 2009).

Precisely controlling the macro- and micro-architecture of the scaffold and hence fulfilling a custom design with complex anatomic shapes are of significant importance for clinical applications of the scaffold. In order to achieve extensive and detailed control over scaffold architecture, designed manufacturing techniques, usually referring to as solid free-form fabrication or rapid prototyping (RP) technologies, are introduced into the tissue engineering field and have been developed for scaffold manufacture.

RP comprises a group of techniques that can generate a physical model directly from computer-aided design data or data provided by computer-based medical imaging technologies in a layer-by-layer manner, and each layer is the shape of the cross-section of the model at a specific level (Hutmacher *et al.* 2004; Yeong *et al.* 2004; Naing *et al.* 2005). More and more RP techniques have been investigated, developed and commercialized for tissue engineering scaffold fabrication using different biomaterials, especially biodegradable materials, as raw materials. Based on the working principle, RP techniques can be divided into several categories: laser polymerization-based techniques, such as stereolithography; nozzle deposition-based techniques, such as fused deposition modelling; and powder-based techniques, such as selective laser sintering (SLS) and three-dimensional printing (Peltola *et al.* 2008; Hollister 2009*b*). Each category of techniques is suitable for a specific form of material and has their own advantages and disadvantages.

Despite the increasing interest in and progress of RP techniques in tissue engineering, engineering of complex and multifunctional features with optimal design, bioactive component and vascular networks is still considered as a challenge for further improvement. Therefore, there have been many attempts in tackling these problems. Finite element analysis was used to study the interactions between scaffold pore morphology, mechanical stimuli developed at the cell microscopic level and culture conditions applied at the macroscopic scale and the fabrication parameters could be optimized through design of experiments for obtaining high-quality scaffolds (Kim & Cho 2009; Olivares *et al.* 2009; Duan *et al.* 2008*b*; Wiria *et al.* 2010). Growth factors such as vascular endothelial growth factor (VEGF) and bone morphogenetic protein (BMP) were incorporated usually by the physical adsorption method onto the scaffold surface so as to enhance the vascularization and bone formation (Ma *et al.* 2009; Yang *et al.* 2009). In addition, new biomaterials and fabrication techniques are under investigation in order to extend the existing list of biomaterials and production methods and even to realize organ printing using scaffold-free cellular spheroids for complex organ constructs (Melchels *et al.* 2009; Mironov *et al.* 2009).

From material point of view, bone can be considered as a nanocomposite consisting of organic matrix (mainly collagen) and inorganic nanofillers (mainly bone apatite), which are inserted in a parallel way into the collagen fibrils (Fratzl *et al.* 2004; Murugan & Ramakrishna 2005). For bone tissue repair or regeneration, nanocomposites consisting of biodegradable polymer matrix and nanosized fillers such as bioceramic, bioglass and carbon nanotube are considered promising strategy to biomimic the hierarchical structure of bone (Chesnutt *et al.* 2009; Meng *et al.* 2009; Li *et al.* 2010). Some researchers have incorporated nanosized bioactive ceramics in RP technique produced scaffolds and the incorporation was normally achieved by dry-blending of polymer with bioceramic powder (Heo *et al.* 2009*a*). Nanocomposite scaffolds with controlled architecture, better osteoconductivity and improved properties, such as mechanical properties, surface properties and degradation rate could therefore be achieved. Using RP technique for scaffold construction, there is also a need to further combine nanocomposites, bioactive factors and cells for bone tissue regeneration.

In this paper, the research, which was based on our previous work and comprised our current work, to integrate the advanced manufacturing technique for complex structure scaffolds, nanocomposite and growth factor delivery for bone tissue engineering is reported. Calcium phosphate (Ca–P)/poly(hydroxybutyrate-co-hydroxyvalerate) (PHBV) nanocomposite scaffolds based on Ca–P/PHBV nanocomposite microspheres were fabricated using a modified SLS machine. The nanocomposite scaffolds produced were subjected to surface modification by entrapment of gelatin and immobilization of heparin. Recombinant human bone morphogenetic protein-2 (rhBMP-2) was incorporated in the scaffolds using its binding affinity with heparin which also controlled the rhBMP-2 release behaviour for the osteogenesis differentiation of mesenchymal stem cells (MSCs).

2. MATERIAL AND METHODS

2.1. Fabrication of Ca–P/PHBV nanocomposite microspheres

The experiments, from Ca–P nanoparticle synthesis to Ca–P/PHBV nanocomposite scaffold fabrication, are schematically illustrated in figure 1.

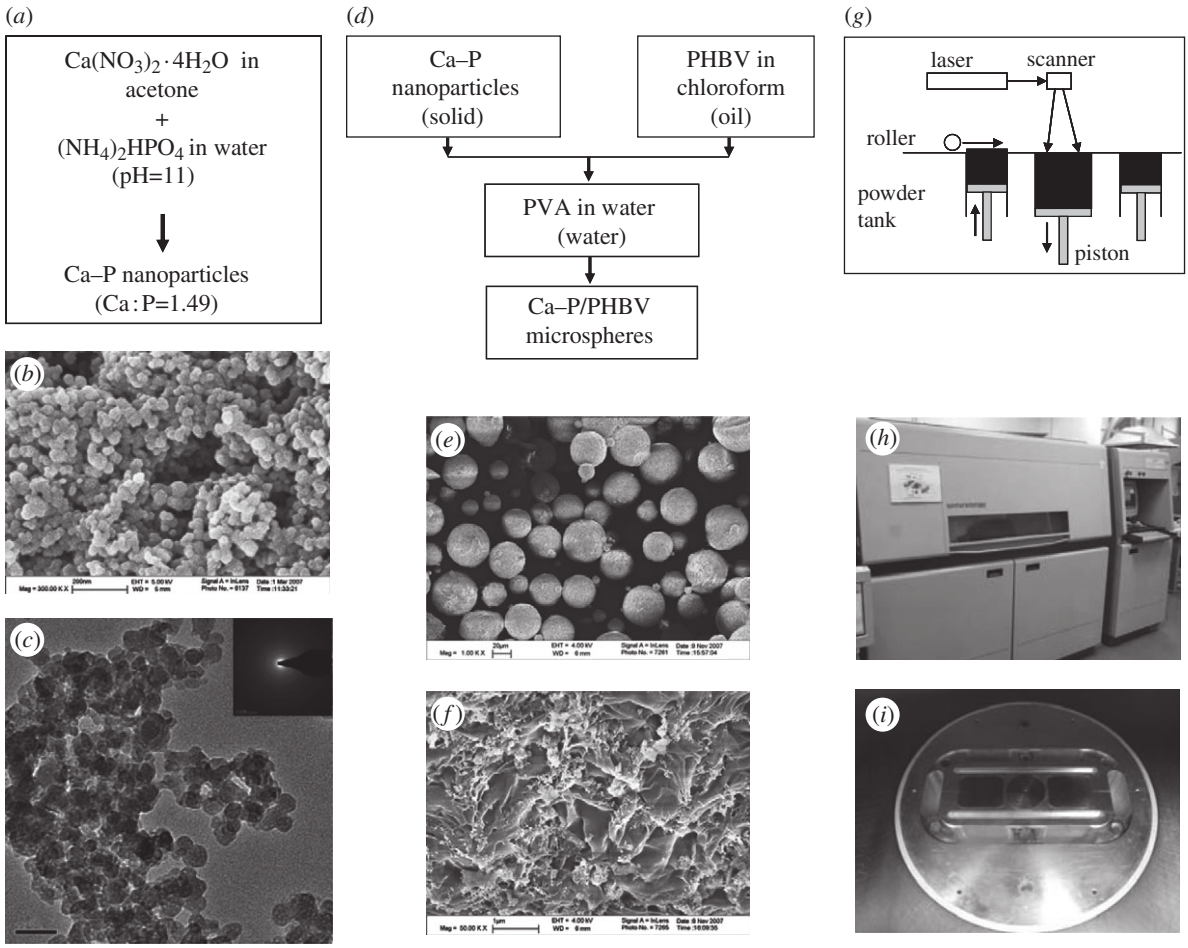

Figure 1. Schematic illustration of the processing for Ca–P/PHBV nanocomposite scaffold fabrication. Left panel: (*a*) synthesis of Ca–P nanoparticles based on Ca and P sources and at pH 11, (*b*) Ca–P nanoparticles observed under SEM, (*c*) TEM image and SAD pattern of Ca–P nanoparticles. Middle panel: (*d*) fabrication of Ca–P/PHBV microspheres using S/O/W emulsion–solvent evaporation method, (*e*) Ca–P/PHBV nanocomposite microspheres, (*f*) high magnification view of the Ca–P nanocomposite microsphere surface. Right panel: (*g*) schematic illustration for the principle of SLS, (*h*) a Sinterstation illustration 2000 SLS system, (*i*) the miniature sintering platform for modified Sinterstation 2000 SLS system.

Ca–P nanoparticles were firstly synthesized in-house by rapid mixing of $Ca(NO_3)_2 \cdot 4H_2O$ (Uni-Chem, Orientalab, China) acetone solution with $(NH_4)_2HPO_4$ (Uni-Chem, Orientalab) aqueous solution. With sizes in the range of 10–30 nm, the obtained Ca–P nanoparticles were amorphous and had a Ca : P molar ratio of about 1.5 (Duan *et al.* 2008*a*). Owing to the consideration for cost, two types of PHBV were used for producing Ca–P/PHBV nanocomposite scaffolds for different studies in the current research. For non-biological studies that required the use of a relatively large amount of PHBV, Ca–P/PHBV nanocomposite scaffolds used PHBV that was purchased from Tianan Biologic Material, China, and contained 2.9 mol% of 3-hydroxyvalerate (HV). For biological studies, Ca–P/PHBV nanocomposite scaffolds were fabricated using PHBV produced by ICI, UK, and contained 12 mol% of HV. SLS required powdered raw materials. Therefore, Ca–P/PHBV nanocomposite microspheres containing Ca–P nanoparticles were fabricated using a solid-in-oil-in-water (S/O/W) emulsion solvent evaporation method (Duan *et al.* 2008*a*). The Ca–P/PHBV nanocomposite microspheres produced had an average diameter of 46.34 μm, as was measured by particle sizer (Mastersizer 2000 instrument, Malvern, UK). Their Ca–P content was 12.9 wt% Ca–P (targeting at 15%), as was determined through thermal gravimetric analysis (TGA). Pure PHBV polymer microspheres were also produced using the oil-in-water (O/W) emulsion/solvent evaporation method.

2.2. Three-dimensional scaffold design and fabrication

A modified Sinterstation 2000 system (3D Systems, Valencia, CA, USA) was used for the SLS of scaffolds or porous structures. The modification of the SLS machine and use of the modified machine for building scaffolds was reported previously (Zhou *et al.* 2008). In order to demonstrate the capability of SLS in constructing porous structures/scaffolds of complex shapes and architecture, three complex models designed by Hart (2009; figure 2*a*) were employed for producing porous structures via SLS. Furthermore, a real human proximal femoral condyle model was built from computer tomography (CT) scans and then processed to a porous scaffold model with a pore size of 2 mm and a

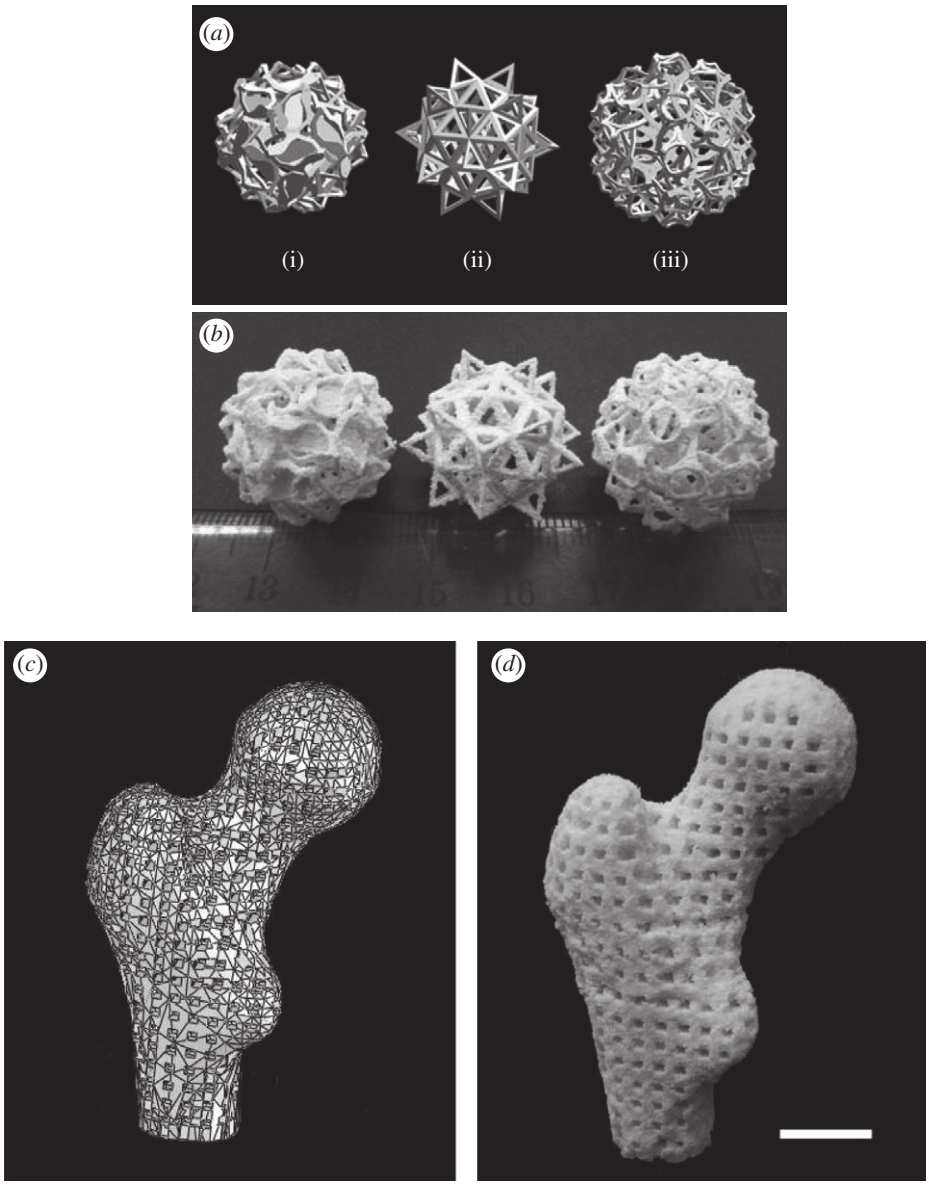

Figure 2. (*a*) Complex models designed and shared by Hart (2009): (i) *salamanders*, (ii) *elevated icosidodecahedron*, (iii) *snarl*; (*b*) sintered Ca–P/PHBV nanocomposite porous structures based on the Hart models; (*c*) three-dimensional model of a human proximal femoral condyle reconstructed from CT images and then processed into porous scaffold using cubic cells; (*d*) sintered Ca–P/PHBV nanocomposite proximal femoral condyle scaffold. (The real size of the sintered proximal femoral condyle scaffold was 40% of the design model.) Scale bar, 1 cm.

strut size of 2.5 mm (figure 2*c*). This human proximal femoral condyle scaffold model was converted into STL file (STL being derived from the name stereolithography) and transferred into the modified SLS machine. An actual Ca–P/PHBV scaffold, representing a scale-down to 40 per cent of the human proximal femoral condyle scaffold model, was produced via SLS. For cytocompatibility and surface modification studies, two porous scaffold models with three-dimensional periodic architectures were designed using SolidWorks (figures 3*a* and 4*a*). The designs were exported into an STL format and transferred to the modified SLS machine for scaffold production. According to our previous SLS optimization results, the laser power was set to be 15 W and the scan spacing and layer thickness were 0.1 mm and 0.1 mm, respectively. The part bed temperature, scan speed and roller speed were fixed at 35°C, 1257 mm s^{-1} and 127 mm s^{-1}, respectively.

2.3. Surface modification

Rod-shaped Ca–P/PHBV nanocomposite scaffolds were designed and fabricated via SLS (figure 4*a*). The surface modification of these scaffolds was conducted in two steps: physical entrapment of gelatin and heparin immobilization. The physical entrapment of gelatin on scaffolds was achieved by immersing sintered Ca–P/PHBV scaffolds (two layers, approx. 70 mg per each scaffold) into a gelatin (Sigma, USA) solution with a miscible mixture of 2,2,2-trifluoroethanol (TFE; Acros, Belgium) and distilled water (TFE : water = 30 : 70) at room temperature for 6 h. After the treatment, the modified scaffolds were rinsed in distilled water for three times

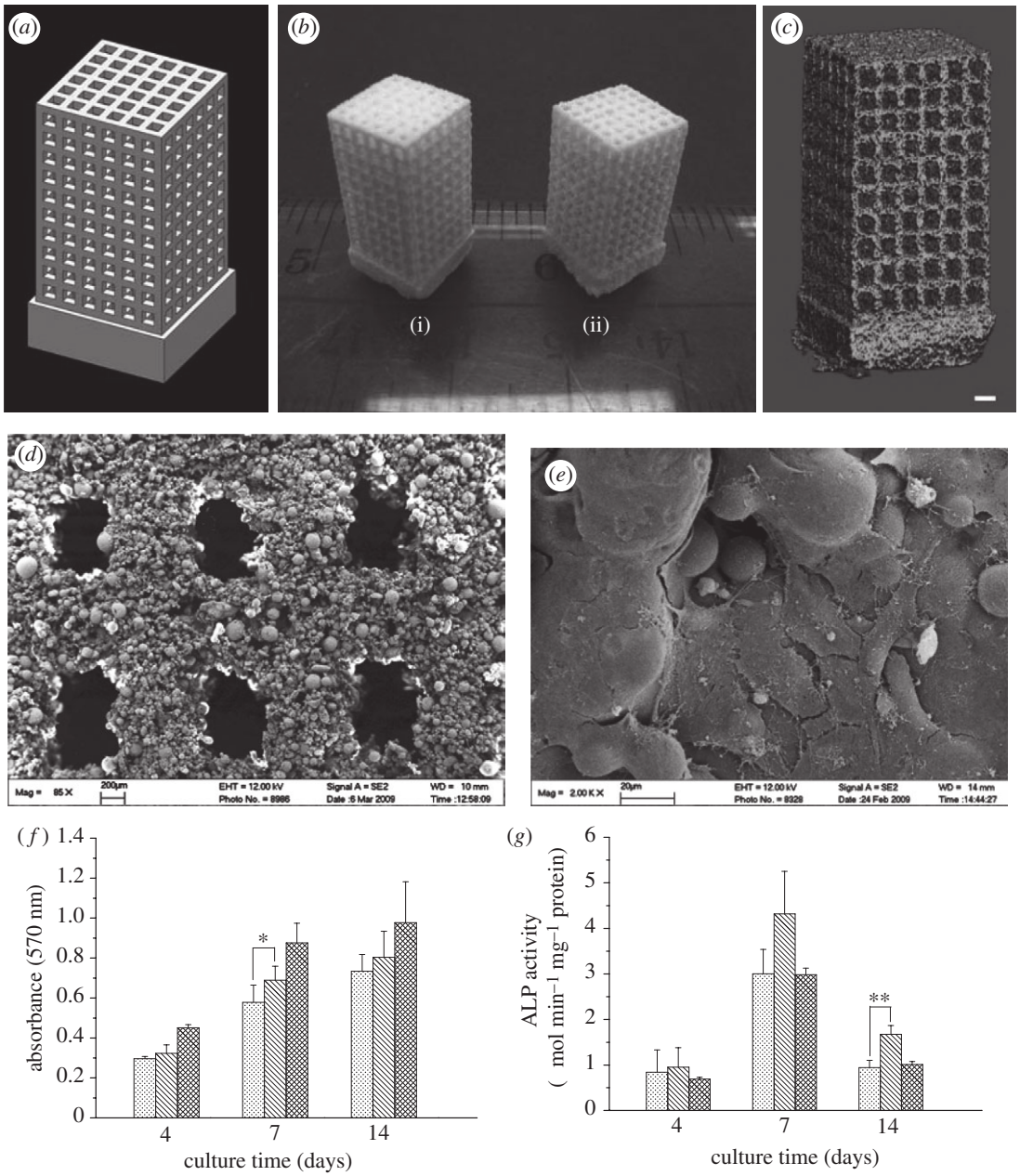

Figure 3. Sintered PHBV polymer scaffolds and Ca–P/PHBV nanocomposite scaffolds for cytocompatibility tests. (*a*) Schematic of the computer-aided design model in trimetric view; (*b*) sintered scaffolds: (i) PHBV polymer scaffold, and (ii) Ca–P/PHBV nanocomposite scaffold; (*c*) micro-CT image of Ca–P/PHBV nanocomposite scaffold; (*d*) SEM image of one layer of sintered Ca–P/PHBV nanocomposite scaffold; (*e*) morphology of SaOS-2 cells cultured for 7 days on Ca–P/PHBV nanocomposite scaffold; (*f*) SaOS-2 cell proliferation determined by MTT assay ($*p < 0.05$); (*g*) ALP activity of SaOS-2 cells ($**p < 0.01$); (*f*,*g*) bar with dots, PHBV; bar with lines, Ca–P/PHBV; bar with crosses, control.

to remove non-entrapped gelatin and dried at room temperature. The gelatin amount entrapped on the scaffold surface was determined quantitatively using bicinchoninic acid (BCA; Pierce, Rockford, IL, USA) kit assay. For heparin immobilization, gelatin-entrapped Ca–P/PHBV scaffolds were first prewetted in 2-(*N*-morpholino) ethanesulphonic acid (MES) buffer solution (0.1 M, pH 5.6; Fluka, USA) for 30 min at room temperature. 3 mg of heparin (Mw 17 000, activity 170USP units mg^{-1}; Sigma, USA) were dissolved in 1 ml MES buffer solution (0.1 M, pH = 5.6) containing 2 mg *N*-hydroxysuccinimide (NHS; Sigma, USA) and 1.2 mg 1-ethyl-3-(3-dimethylaminopropyl)-carbodiimide hydrochloride (EDC; Sigma, USA). After 4 h of activation at room temperature, the prewetted scaffolds were soaked in the activated heparin solution in MES buffer for another 4 h and then extensively washed with phosphate-buffered saline (PBS) and dried over night at room temperature. The stability of immobilized heparin was studied by immersing heparin-conjugated scaffolds in PBS solution at 37°C up to 14 days. The remaining heparin on scaffolds was qualitatively measured using the toluidine blue method (Chung *et al.* 2006). Scaffolds without surface modification were used as control for the heparin stability tests. For wettability assessment, PHBV films were produced using the solvent-casting method. Briefly, PHBV–chloroform solution was cast into a glass Petri dish and placed in a fume hood at

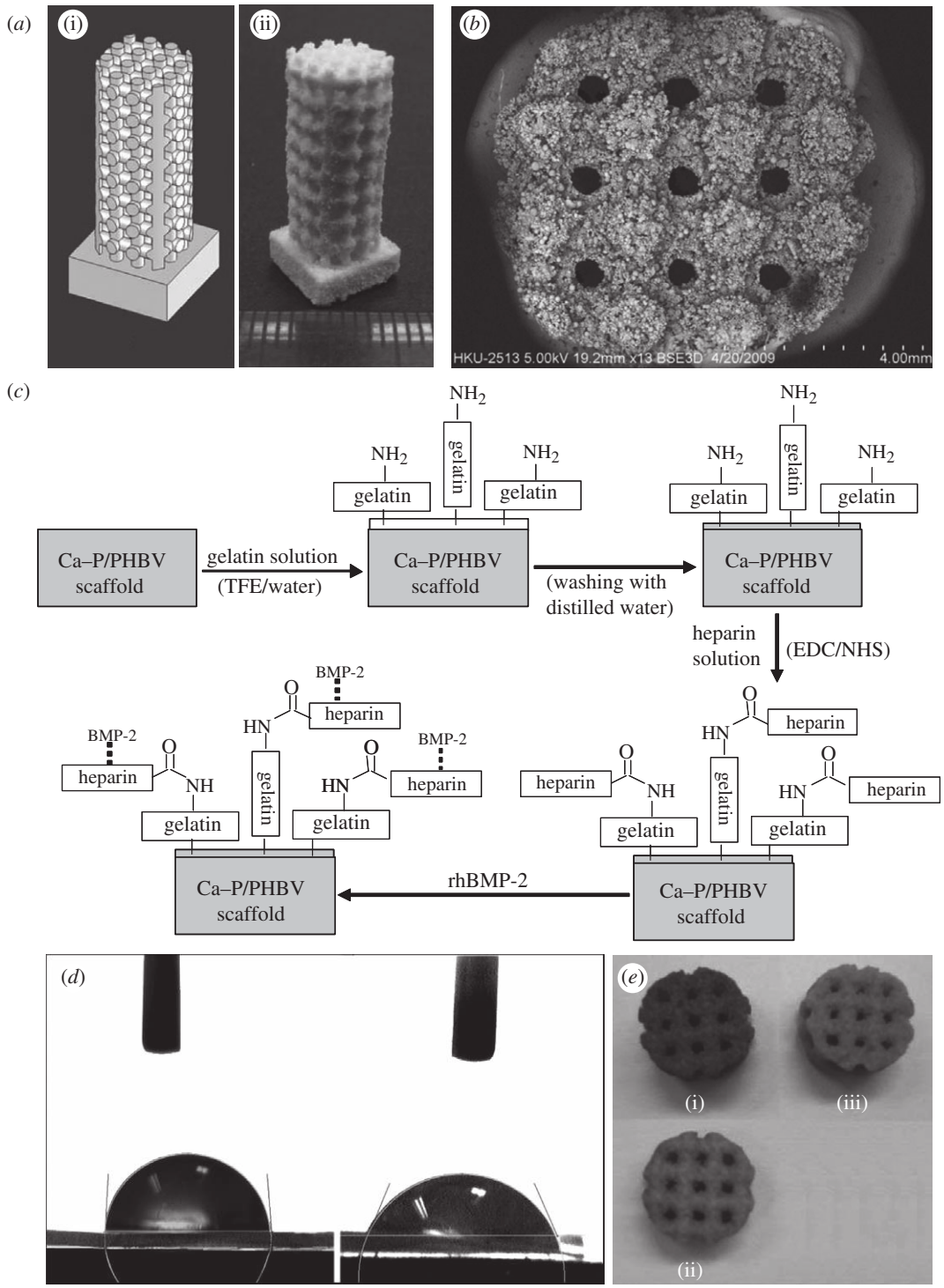

Figure 4. (*a*) Ca–P/PHBV scaffolds for surface modification: (i) design model and (ii) sintered Ca–P/PHBV nanocomposite scaffold; (*b*) SEM image of sintered Ca–P/PHBV nanocomposite scaffold (top view); (*c*) illustration of physical entrapment of gelatin and immobilization of heparin on the surface of sintered Ca–P/PHBV nanocomposite scaffold and the binding strategy of rhBMP-2; (*d*) contact angle images for PHBV film (left) and surface modified PHBV film (right); (*e*) images of Ca–P/PHBV nanocomposite scaffolds after toludine blue staining: (i) scaffold with immobilized heparin in the as-produced state, (ii) scaffold with immobilized heparin after 14-day immersion in PBS, and (iii) scaffold control sample without immobilized heparin.

room temperature for the slow evaporation of chloroform. After further vacuum drying, PHBV film was collected and cut into square samples of the dimensions 1 cm × 1 cm. The surface modification of solvent cast PHBV films adopted the same procedure as described above.

Ca–P/PHBV nanocomposite scaffolds with and without surface modification were loaded with 5 μg rhBMP-2 by dripping 50 μl rhBMP-2 solutions with 20 mM glacial acetic acid and 0.1 per cent BSA. The rhBMP-2 loaded scaffolds were used for studying osteogenic differentiation of C3H10T1/2 MSCs.

2.4. Characterization

The morphology of sintered scaffolds (both bar-shaped and rod-shaped) was examined using scanning electron

microscopes (LEO 1530 FE-SEM or Hitachi S-3400N SEM) and the porosity of scaffolds was measured using a density kit and an electronic balance on the basis of Archimedes principle (Karageorgiou & Kaplan 2005). For micro-CT imaging, sintered Ca–P/PHBV scaffolds were scanned with a desktop fan beam type micro-CT system (microCT20, Scano Medical AG, Bassersdorf, Switzerland). For wettability assessment, a contact angle machine (SL200B, Solon Tech, Co. Ltd., Shanghai, China) equipped with an image analysing system was used and contact angles were measured at room temperature employing the sessile drop technique.

2.5. Cell culture

Human osteoblast-like cell line (SaOS-2) and murine pluripotent mesenchymal cell line, C3H10T1/2, were cultured, respectively, in Dulbecco's Modified Eagle Medium (DMEM, Gibco, USA) containing 10 per cent foetal bovine serum (Biowest, France), 100 U ml^{-1} penicillin–streptomycin, 4 $\mu g\,ml^{-1}$ fungizone, and 2 mM L-glutamine (Invitrogen, USA). The culture medium was replaced every 2 days and cultures were maintained in a humidified incubator at 37°C with 5 per cent CO_2. After reaching about 80 per cent confluence, the cells were digested and subcultured using 0.25 per cent (w/v) trypsin-ethylenediamineteraacetic acid (Invitrogen, USA). The resulting cells in a suspension were then seeded separately onto two-layer scaffolds (bar-shaped scaffolds, as shown in figure 3*b*), which had been sterilized by ^{60}Co γ-irradiation at a dose of 25 kGy. For control experiments, polystyrene tissue culture plates (TCPs) were used. The cells were seeded onto each sample by dripping a cell suspension in 24-well plate and then the culture wells were filled with 1 ml of culture medium after 2 h in the incubator.

2.6. Cell proliferation

Cell proliferation was determined using 3-(4,5-dimethylthiazol-2-yl)-2,5-diphenyltetrazolium bromide (MTT) assay. The culture medium was removed and cell-scaffold constructs were washed with PBS to remove non-adhering cells. Culture medium with MTT solution (5 mg ml^{-1} in PBS) was added to each cell-scaffold sample, followed by incubation for 4 h at 37°C. After removal of the medium, the formed formazan crystals were dissolved in dimethyl sulphoxide and the absorbance was measured using a microplate spectrophotometer (UVM 340, Asys HiTech GmbH, Austria) at a wavelength of 570 nm.

2.7. Osteogenic differentiation

For determining the osteogenic capacity of C3H10T1/2 cells, the cells grown on TCPs were cultured in basal medium supplemented with 10 nM dexamethasone, 0.05 mM L-ascorbic acid, 0.01 mM β-glycerophosphate (Sigma) and 1000 ng ml^{-1} recombinant human bone morphogenetic protein-2 (rhBMP-2) (Shanghai Rebone Biomaterials Co. Ltd, China). The medium was refreshed every 2–3 days. After 21 day of osteogenic induction, C3H10T1/2 cells were stained with the alkaline phosphatase (ALP) leucocyte kit (Sigma, USA) according to the provided protocol. The calcium deposition was stained with 1 per cent Alizarin Red S after fixation by 10 per cent neutralized formalin.

Both SaOS-2 cells and C3H10T1/2 cells were seeded separately on different scaffolds and cultured up to 21 days. The ALP activity of SaOS-2 cells and C3H10T1/2 cells on these scaffolds was quantitatively measured. The cells were lysed in lysis buffer containing 0.1 per cent (v/v) Triton X-100, 1 mM $MgCl_2$ and 20 mM Tris, which was followed by a freezing and thawing process to further disrupt the cell membranes. The lysate was mixed with ALP substrate solution containing *p*-nitrophenyl phosphate (Sigma, USA) at 37°C for 30 min. The reaction was stopped by the addition of 3 N NaOH and then the production of *p*-nitrophenol in the presence of ALPase was measured by monitoring the absorbance of the solution at a wavelength of 405 nm using a microplate reader. The total protein content was determined using BCA assay kit with bovine serum albumin as a standard and the ALP activity was expressed as micromoles of *p*-nitrophenol formation per milligram of total proteins in 30 min.

2.8. Reverse transcriptase–polymerase chain reaction (RT–PCR) analysis

After 21-day induction in the osteogenic medium, total RNA was first isolated using an Absolutely RNA Microprep Kit (Stratagene, USA) according to the manufacturer's protocol. The mRNA was reverse transcribed to complementary DNA (cDNA) using a Transcriptor First Strand cDNA Synthesis Kit (Roche Diagnostics, Germany) and 2 μL of cDNA template from each RT reaction were subjected to PCR reactions using FastStart Taq DNA polymerase (Roche Diagnostics, Germany) run in a Bio-RAD iCycler System (Bio-RAD, USA). Thirty-five cycles of PCR was performed and the products were electrophoresis on a 1.5 per cent agarose gel and visualized with ethidium bromide staining. Oligonucleotide primers were: collagen type I (Col1A1) (5′ CTGACCTTCCTGCGCCTGATGTCC3′; 5′ GTCTGGGGCACCAACGTCCAAGGG3′); ALP (5′ACTGCTGATCATTCCCACGTT3′; 5′ GAAC AGGGTGCGTAGGGAGA3′); osteocalcin (OCN) (5′ CAAGTCCCACACAGCAGCTT3′; 5′ AAAGCC GAGCTGCCAGAGTT3′) and glyceraldehyde-3-phosphatedehydrogenase (GAPDH) (5′ GGCAAATTC AACGGCACAGTC3′; 5′ AAGCAGTTGGTGGTGC AGGA3′), which served as housekeeping gene.

2.9. Cell morphology observation by SEM

The cell-scaffold constructs were harvested, washed twice with PBS, and subsequently fixed with 2.5 per cent glutaraldehyde at 4°C for 4 h. After washing with cacodylate buffer containing 0.1 M sucrose, they were dehydrated through a series of graded alcohol solutions and dried in a critical point dryer using liquid carbon dioxide as transition fluid. The cell-scaffold samples were then glued onto aluminium stubs and sputter-coated with a thin layer of gold for SEM observation.

2.10. Statistical analysis

All quantitative data were collected from triplicate samples and expressed as the mean ± s.d. Statistical analysis was conducted using ANOVA with a Scheffé test. A value of $p < 0.05$ was considered to be statistically significant and $p < 0.01$ remarkably significant.

3. RESULTS

3.1. Design and fabrication of scaffolds and complex porous structures

As a family member of RP techniques, SLS employs a CO_2 laser to selectively sinter thin layers of powdered polymers or their composites, forming solid three-dimensional objects. Therefore, Ca–P/PHBV nanocomposite microspheres were first fabricated and served as raw materials for the scaffold sintering processes. With sizes in the range of 10–30 nm, the Ca–P nanoparticles synthesized in-house (figure 1*b*,*c*) were amorphous and had a Ca : P molar ratio of about 1.49. Ca–P/PHBV nanocomposite microspheres based on Ca–P nanoparticles and biodegradable PHBV matrix were fabricated using S/O/W emulsion–solvent evaporation method. PHBV microspheres were also made. While most Ca–P nanoparticles were encapsulated in the PHBV matrix in Ca–P/PHBV microspheres (Duan *et al.* 2008*a*) as shown in figure 1*f*, some Ca–P nanoparticles adhered to the surface of Ca–P/PHBV microspheres. For sintering Ca–P/PHBV nanocomposite scaffolds, a miniature sintering platform containing two small powder supply tanks and one small build cylinder tank was designed and installed in the build cylinder of existing Sinterstation 2000 system, as shown in figure 1*h*,*i* (Zhou *et al.* 2008). This SLS machine modification significantly reduced consumption of raw, powdered materials for scaffold fabrication.

Based on the factorial design methodology, a systematic study of the effects of various SLS parameters on the quality of sintered scaffolds was conducted and optimized scaffold fabrication process via SLS was established (Duan *et al.* 2008*b*). As a demonstration of the capability of the SLS technique in producing scaffolds of complex shapes and architectures, two types of RP models were used for SLS fabrication of porous structures and usable scaffolds in the current research: (i) models designed through computer software; and (ii) a model based on a modern medical imaging technique. As shown in figure 2*a*, three complex models designed and shared by Hart (2009) were employed. Based on these models, porous structures, as shown in figure 2*b*, were successfully made using optimized SLS parameters mentioned above. Figure 2*c* exhibits a three-dimensional model of human proximal femoral condyle reconstructed from CT images. The model was processed into a porous scaffold using cubic cells (pore size of 2 mm and strut size of 2.5 mm), converted into STL file and transferred to the modified SLS machine. The size of femoral condyle scaffold was scaled down to 40 per cent in order to save Ca–P/PHBV material and to fit the size of build cylinder tank of the modified SLS machine. The pore size and strut size of the scaled-down femoral condyle scaffold model were 0.8 mm and 1.0 mm, respectively. Again, optimized SLS parameters were used for sintering the femoral condyle scaffold. The sintered porous scaffold, as shown in figure 2*d*, was comparable to the design.

Using optimized SLS parameters, Ca–P/PHBV scaffolds in the shape of bars (figure 3*b*) and rods (figure 4*a*) were fabricated for cytocompatibility study and surface modification study, respectively.

3.2. Cytocompatibility of Ca–P/PHBV nanocomposite scaffolds

A tetragonal scaffold model with three-dimensional orthogonal periodic porous architecture (figure 3*a*) was designed, with the strut size being 0.5 mm and the pore size being 0.8 mm. Both PHBV polymer and Ca–P/PHBV nanocomposite microspheres were successfully sintered into scaffolds (figure 3*b*) for cytocompatibility tests. The scaffolds fabricated had intact structure and good handling stability and hence entrapped microspheres inside the scaffolds, *viz.*, the non-sintered microspheres, could be easily removed by shaking the scaffolds manually. The porosity of sintered PHBV and Ca–P/PHBV scaffolds was measured to be 64.6 ± 2.0 per cent and 62.6 ± 1.2 per cent, respectively, which are larger than the designed value (52.7%). A micro-CT image of sintered Ca–P/PHBV scaffold is shown in figure 3*c*. Apart from the designed macropore structure, micropores between adjacent microspheres were also observed on the sintered struts from the micro-CT image. The general view of a layer of sintered Ca–P/PHBV scaffold is shown as figure 3*d*. It can be seen that the morphology of each layer of the scaffold was well preserved and the pores were clearly identified and comparable to the designed scaffold model.

In the current study, the cytocompatibility tests of both PHBV and Ca–P/PHBV scaffold samples were performed using SaOS-2 cells, a human osteoblast-like cell line. An SEM image of SaOS-2 cells cultured for 7 days on the surface of Ca–PHBV nanocomposite scaffold is presented as figure 3*e*. After 7 days of culture, SaOS-2 cells spread well over the strut surface and showed normal morphology and phenotype, forming subconfluent monolayer. The cellular attachments were characterized by numerous protrusions of filopodia. These filopodia anchored the cells on the strut surface of sintered scaffolds. It was also observed that cells could bridge the neighbouring microspheres on the strut. The proliferation of SaOS-2 cells on PHBV and Ca–P/PHBV scaffolds, as well as on TCPs as control, in terms of the relative absorbance is shown in figure 3*f*. The nanocomposite scaffolds presented increments in the number of viable cells in comparison with the polymer counterparts during the entire cell culture period. As expected, the incorporation of nanosized Ca–P in PHBV to form composite scaffolds significantly promoted cell growth on day 7, showing significant by higher metabolic activity when compared with PHBV scaffolds ($p < 0.05$). The ALP expressed

by SaOS-2 cells seeded on different scaffolds was quantified, as shown in figure 3*g*. The ALP activity on sintered scaffolds, as well as on TCPs, increased from 4-day to 7-day culture and then decreased after day 7. Ca–P/PHBV nanocomposite scaffolds exhibited significantly higher ALP activity than PHBV scaffolds after 14-day culture ($p < 0.01$).

3.3. Surface modification of Ca–PHBV nanocomposite scaffolds

Another three-dimensional periodic porous scaffold model was designed for the surface modification study and is shown in figure 4*a*. The distance between each layer and each pillar in the scaffold was 0.8 mm and the solid pillar was 1 mm in diameter. Figure 4*b* is the top view of sintered Ca–P/PHBV nanocomposite scaffold under SEM. According to the design (figure 4*a*), looking vertically from the top, the pores should assume the square shape. However, because of the 'growth effect' of struts of scaffolds during SLS, the four corners of pores were rounded and pores in the scaffolds appeared to be circular in shape (figure 4*b*).

For surface modification, the physical entrapment technique was employed, which involved the use of a miscible mixture of solvent and non-solvent for PHBV. During the entrapment process, PHBV matrix swelled but did not dissolve in the gelatin solution. After the scaffold was removed from gelatin solution and immersed in distilled water, which was non-solvent for the PHBV polymer, the surface rapidly shrank and gelatin molecules on the polymer surface were entrapped (Liu *et al.* 2005; Cai *et al.* 2007). The amount of entrapped gelatin was quantitatively measured by BCA kit was determined to be $1955.8 \pm 62.1\ \mu g$ per scaffold. The entrapment of gelatin molecules introduced on strut surfaces amino groups, which could be further used for the conjugation of heparin, as illustrated in figure 4*c*. Heparin was subsequently immobilized onto the gelatin-entrapped scaffold surface based on standard carbodiimide chemistry (Chung *et al.* 2006; Jeon *et al.* 2007). The amount of immobilized heparin was quantitatively determined to be $41.78 \pm 0.39\ \mu g$ per scaffold using the dye-binding-based toluidine blue assay.

Solvent cast PHBV films were used instead of scaffolds for contact angle measurement because of the high porosity of the scaffolds. Distilled water was used as the test liquid and drops of the water were placed on PHBV films with and without surface modification. As shown in figure 4*d*, the contact angle for PHBV film before surface modification was large, being $93.61 \pm 1.85^\circ$. It decreased to $72.06 \pm 0.89^\circ$ after gelatin-entrapment and heparin immobilization. The surface modification had resulted in better wettability of PHBV and hence the scaffolds.

The change of amounts of immobilized heparin on scaffolds, which reflected the stability of immobilized heparin on the scaffolds, during scaffold immersion in PBS was qualitatively measured using the toluidine blue method. Figure 4*e* showed the change of immobilized heparin with immersion time. After 14-day immersion in PBS solution, the amount of heparin decreased from 41.78 ± 0.39 to $22.33 \pm 0.68\ \mu g$ per scaffold. However, the remaining immobilized heparin was still visible after toluidine blue staining, while the control samples (scaffolds without surface modification) could only absorb toluidine blue and show light blue colour (figure 4*e*).

3.4. Osteogenic differentiation of C3H10T1/2

Derived from mouse embryos, C3H10T1/2 cells were shown to have similar phenotypic and functional characteristics with primary bone marrow-derived MSCs (Zhao *et al.* 2009). Under the stimulation of BMPs and specific inductions, C3H10T1/2 cells acquire osteoblastic phenotype and develop into osteoblasts (Shea *et al.* 2003; Kim *et al.* 2009). In the current study, the osteogenic differentiation capacity of C3H10T1/2 cells was first evaluated in osteogenic differentiation medium with and without rhBMP-2. After 21-day osteogenic induction, ALP was expressed in rhBMP-2 treated cultures (figure 5*a*). For the accumulation of calcium deposition, C3H10T1/2 cells in rhBMP-2 added medium showed positive staining result as assessed by Alizarin Red S staining (figure 5*b*), indicating their differentiation potential towards osteogenic fate. However, no distinct osteogenic phenotype was observed for C3H10T1/2 cells cultured in basal medium without osteogenic inducing factors (data not shown in this paper).

C3H10T1/2 cells were cultured on different scaffolds, namely, bare Ca–P/PHBV nanocomposite scaffolds with and without rhBMP-2 adsorption and the surface-modified Ca–P/PHBV nanocomposite scaffolds loaded with rhBMP-2, up to 21 days in osteogenic medium. The cellular adherence and spread of C3H10T1/2 cells on surface modified Ca–P/PHBV nanocomposite scaffold was examined using SEM after 21-day culture in osteogenic medium, showing proliferating cells all over the surface of the scaffolds. Interestingly, the biomimetic deposition of an apatite layer on some microspheres of the strut surface was also observed, and there appeared to be close interaction between the cells and apatite-covered micropsheres (figure 5*d*). For cell cultures on different scaffolds in the osteogenic medium, as shown in figure 5*e*, the ALP activity of cells on scaffolds loaded with rhBMP-2 was significantly increased compared with that on scaffolds without rhBMP-2, indicating the important role of rhBMP-2 in osteogenic differentiation. Surface-modified scaffolds loaded with rhBMP-2 showed statistically higher ALP activity than scaffolds with simple adsorption of rhBMP-2 did ($p < 0.01$ on day 7 and 21; $p < 0.05$ on day 14). The expression of genes related to the osteoblastic phenotype was examined using RT–PCR in order to investigate the binding effect of surface modified scaffolds on the (controlled) rhBMP-2 release from scaffolds as well as further gene expression. Expression of collagen IA1 was slightly higher in the cells grown on surface- modified scaffolds loaded with rhBMP-2 than in the cells grown on the scaffolds without surface modification or surface-modified scaffolds without rhBMP-2. Obviously, the heparin immobilization and

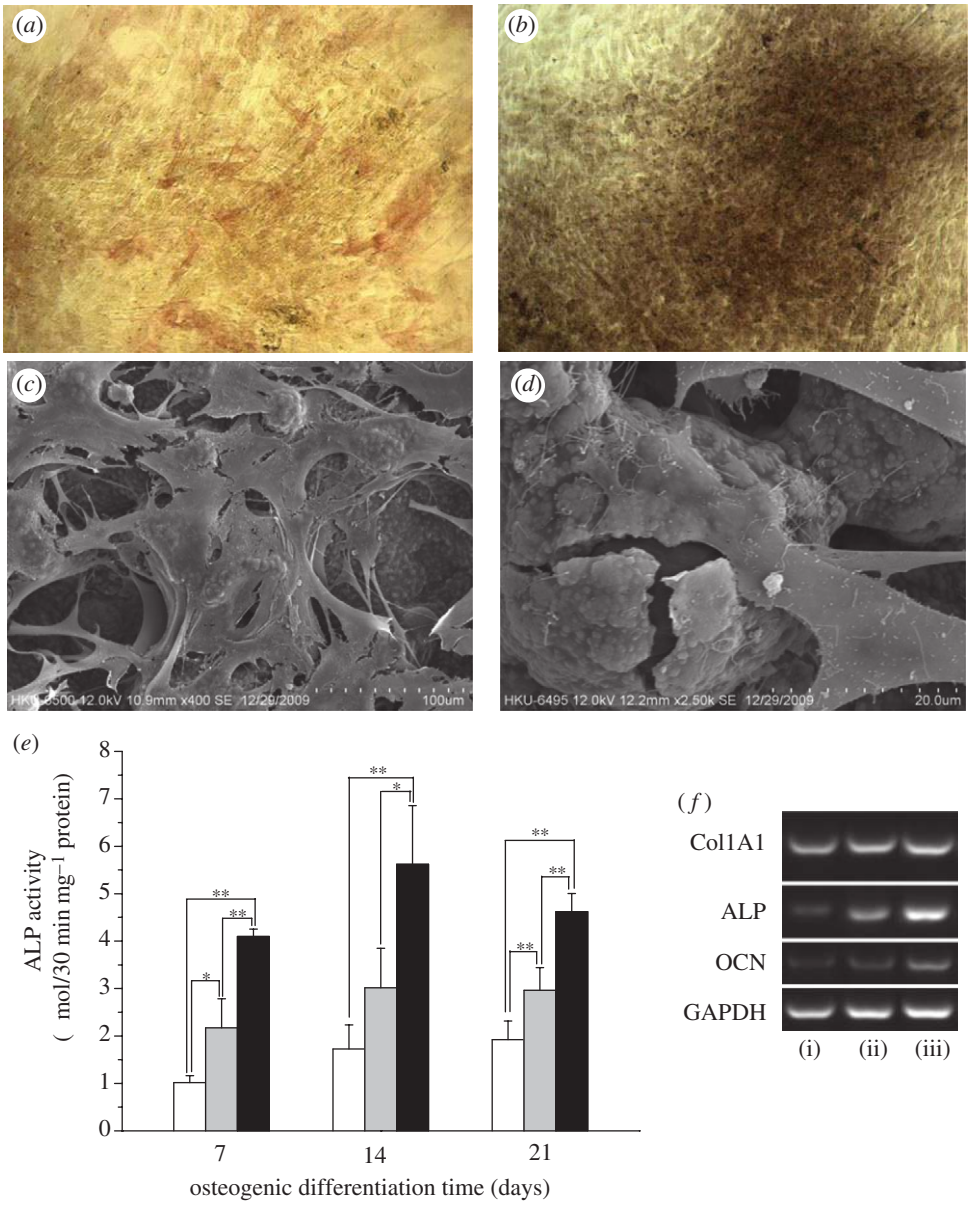

Figure 5. (*a*,*b*) Osteogenic differentiation of C3H10T1/2 cells in osteogenic medium with 1000 ng ml^{-1} rhBMP-2 for 21 days, evidenced by (*a*) positive ALP staining and (*b*) calcium deposition stained by Alizarin Red S; (*c*) morphology of C3H10T1/2 cells cultured on surface modified Ca–P/PHBV nanocomposite scaffold for 21 days in osteogenic medium; (*d*) high magnification view showing the interaction between C3H10T1/2 cells and Ca–P/PHBV microspheres in the strut of nanocomposite scaffold; (*e*) ALP activity of C3H10T1/2 cells cultured on different scaffolds in osteogenic medium for 21 days. White bars, Ca–P/PHBV nanocomposite scaffolds; grey bars, Ca–P/PHBV nanocomposite scaffolds with simply adsorbed rhBMP-2; black bars, surface modified Ca–P/PHBV nanocomposite scaffolds loaded with rhBMP-2 (*$p < 0.05$; **$p < 0.01$); (*f*) gene expression of different osteogenic markers after 21-day cell culture for different scaffolds: (i) Ca–P/PHBV nanocomposite scaffolds; (ii) Ca–P/PHBV nanocomposite scaffolds with simply adsorbed rhBMP-2; (iii) surface-modified Ca–P/PHBV nanocomposite scaffolds loaded with rhBMP-2. (Collagen IA1 (Col1A1); alkaline phosphatase (ALP); osteocalcin (OCN); glyceraldehyde-3-phosphatedehydrogenase (GAPDH).)

incorporation of rhBMP-2 on Ca–P/PHBV nanocomposite scaffolds enhanced the ALP and OCN gene expression (figure 5*f*).

4. DISCUSSION

RP techniques are matured manufacturing technologies widely employed in traditional industries such as automobile industry and telecommunication (phone) industry during the design process. They were first borrowed and used by the medical device industry to produce accurate models or prosthesis for surgical planning and simulation (Berry *et al.* 1997; Petzold *et al.* 1999). With the emergence and development of tissue engineering, various biomaterials and RP techniques are being investigated to specifically fabricate porous scaffolds with different architectures and properties, targeting at the regeneration of different tissues such as bone, cartilage, blood vessel, spinal cord, etc. (Lopez-Heredia *et al.* 2008; Xu *et al.* 2008; Woodfield *et al.* 2009; Silva *et al.* 2010). Furthermore, complex

organ regeneration can potentially benefit from RP techniques with the fabrication/formation of functionally graded scaffolds or cell printing based on tissue spheroids (Leong *et al.* 2008; Mironov *et al.* 2009). The application of RP techniques in the tissue engineering field can produce custom-tailored scaffolds to match the patient's needs and can also allow the precise control of scaffold geometry, architecture and porosity. The current study has clearly demonstrated the applicability and capability of one type of RP technology, the SLS technique, for fabricating useful/usable tissue engineering scaffolds.

For bone tissue repair and regeneration, porous and non-porous composites based on biodegradable polymer and osteoconductive calcium phosphate are promising materials because of the introduction of osteoconductive bioceramic. A number of research groups have developed various bioceramic/polymer composite scaffolds using different RP techniques (Ang *et al.* 2002; Liu *et al.* 2007; Wiria *et al.* 2007; Heo *et al.* 2009*b*). During their processes, in general, dry-blending was used to mix polymer granules and bioceramic powders. The mixtures were then either extruded or sintered to form scaffolds according to the designs. Dry-blending has advantages and disadvantages in forming raw materials for RP techniques and one obvious disadvantage is the non-homogeneous distribution of fine bioceramic particles in RP-produced scaffolds.

In the current study, PHBV polymer microspheres and Ca–P/PHBV nanocomposite microspheres based on PHBV matrix and Ca–P nanoparticles as raw materials for SLS were first fabricated (figure 1*a–f*), instead of using commercial polymer powders and polymer/ceramic blends. Ca–P nanoparticles could be homogeneously distributed in the composite microspheres (Duan *et al.* 2008*a*) or on the microsphere surface when the bioceramic content was high. Another advantage of the current approach is that some drugs or even biomolecules could also be incorporated into the microspheres (and hence the scaffolds after SLS) in order to form multi-functional nanocomposite scaffolds and improve their bioactivity (Duan & Wang 2008). In scaffold fabrication, the commercial SLS machine was modified, using a miniature platform for sintering in order to minimize raw consumption (figure 1*g–i*). This strategy is important as currently most materials for tissue engineering scaffolds are still expensive or the materials are only available in small quantities with the laboratory-scale production. In the current study, two types of PHBV, *viz.*, PHBV with a lower HV content from Tianan (China) and PHBV with a higher HV content from ICI (UK), were used for producing nanocomposite scaffolds for non-biological studies and biological studies, respectively. Both types of PHBV can be successfully fabricated into Ca–P/PHBV nanocomposite microspheres and subjected to sintering process using the optimized SLS parameters. Scaffolds made of different PHBV could have differences in mechanical properties but the differences are not expected to be large.

For the demonstration purpose, both computer-designed models and a model reconstructed from CT images were used for fabricating scaffolds and porous structures of complex shape and architecture via SLS in the current study. Based on these models, robust Ca–P/PHBV nanocomposite scaffolds and porous structures were successfully produced with comparable features (figure 2). It is commonly known that for scaffold fabrication, RP techniques can be integrated with imaging techniques such as CT and magnetic resonance imaging, thereby offering a very useful strategy to precisely produce custom-designed scaffolds for individual patients (Chua *et al.* 2003*a*,*b*; Hutmacher *et al.* 2004). The current study showed that the Ca–P/PHBV nanocomposite microspheres produced in-house could be processed into sintered scaffolds with complex structures for specific bone defect repair. In addition, through controlling the architectures of the scaffolds (pore size, interconnectivity, geometry, etc.), the physical, mechanical and biological properties such degradation rate, scaffold strength and cellular response could be further controlled. In the current study, Ca–P/PHBV nanocomposite scaffolds of bar and rod shapes were designed and fabricated for cytocompatibility study and surface modification study, respectively, as shown in figures 3*a–d* and 4*a*,*b*. The sintered scaffolds had three-dimensional architecture and totally interconnected porous structures.

Both PHBV polymer scaffolds and Ca–P/PHBV nanocomposite scaffolds showed good cytocompatibility and osteoblastic-like cells could well spread over the strut surface of scaffolds and proliferated with increasing culture time. The introduction of Ca–P nanoparticles into scaffolds significantly enhanced cell proliferation after 7-day culture (figure 3*f*) because of the osteoconductivity of these particles. Furthermore, the surface topography change of microspheres from polymer microsphere to nanocomposite microspheres in the strut of scaffolds may have affected the adsorption of various proteins, leading to enhanced cell proliferation (Li *et al.* 2009; Lv *et al.* 2009). Cells on Ca–P/PHBV nanocomposite scaffolds showed significant higher ALP activity expression than on their polymeric counterpart after 14-day culture (figure 3*g*), indicating that Ca–P nanoparticles could facilitate osteogenic differentiation of SaOS-2 cells.

In order to further enhance the functionality of tissue engineering scaffolds, biological signals, especially growth factors, can be incorporated into scaffolds (Biondi *et al.* 2008; Uebersax *et al.* 2009). Ideally, an adequate dose of growth factor(s) should be incorporated according to specific tissue target and be released in a temporal and spatial way for a desired time frame to minimize its/their loss(es) and non-target site release. The generally adopted approaches include direct growth factor delivery by either entrapment or attachment method and gene encoding growth factor delivery (Vasita & Katti 2006; Sokolsky-Papkov *et al.* 2007). However, growth factors are very difficult to be effectively encapsulated within scaffolds that are produced by many RP techniques owing to the application of high temperature and/or polymerization process, which there techniques require. Therefore, the growth factor incorporation and delivery are usually achieved through the simple absorption method (Ma *et al.* 2009; Yang *et al.* 2009). For achieving better

control of the growth factor release behaviour, in the current study, heparin was immobilized on the surface of gelatine-entrapped Ca–P/PHBV nanocomposite scaffolds. Based on carbodiimide chemistry, the entrapped gelatin provided amino group for the conjugation of heparin (figure 4*c*). Heparin, a sulphated polysaccharide belonging to the glycosaminoglycans family, is known to have the binding affinity with a number of growth factors and is thus capable of blocking the degradation of the growth factors and prolonging their release time (Capila & Linhardt 2002; Jiao *et al.* 2007). Therefore, heparin had been immobilized onto the surface of various scaffolds for binding VEGF, BMP and basic fibroblast growth factor (bFGF) (Chung *et al.* 2006; Edlund *et al.* 2008; Ho *et al.* 2009). Based on the specific affinity between heparin and growth factors, the bound growth factors would be released in a sustained manner and would improve angiogenesis or osteogenesis (Edlund *et al.* 2008; Lin *et al.* 2008; Ho *et al.* 2009; Rohman *et al.* 2009). In addition, the surface modification by entrapment of gelatin and immobilization of heparin also significantly improved the wettability of solvent cast PHBV membranes (figure 4*d*), suggesting the improvement of wettability of surface-modified Ca–P/PHBV nanocomposite scaffolds. The cell adhesion in the early stage of cell seeding could therefore be facilitated. The stability of immobilized heparin, as well as its binding strength, is very important because it could further affect the release profile of rhBMP-2. Although about half of immobilized heparin was released in the aqueous PBS solution after 14-day immersion owing to the cleavage of amine bond between carboxylic acid groups in heparin and amino groups in gelatin or the de-entrapment of gelatin, the remaining heparin was still immobilized on the scaffold (figure 4*e*). According to the heparin stability results, the degradation/release/de-entrapment process may last for four weeks or longer. Yoon *et al.* (2006) reported that the bFGF loading amount and load efficiency were gradually increased with increasing amount of immobilized heparin and the sustained release of bFGF was mainly controlled by the amount of bFGF released and free growth factors in the medium, rather than controlled by a diffusion-controlled mechanism. The immobilized heparin with stable conjunction to the scaffolds was beneficial for specifically binding rhBMP-2 and could improve the rhBMP-2 release behaviour, reducing the initial burst release of rhBMP-2.

Pluripotent MSC cell line C3H10T1/2 was employed to investigate their osteogenic differentiation capacity on different scaffolds. It has been reported that C3H10T1/2 cells differentiated along the adipocytic lineage when treated with low concentrations of BMP-2 while osteogenesis was enhanced with higher concentrations of BMP2 (Wang *et al.* 1993). In the current study, the ALP activity assay and mRNA expression results showed that ALP levels were significantly upregulated on surface-modified Ca–P/PHBV scaffolds loaded with rhBMP-2 as compared with scaffolds with simple adsorption of rhBMP-2 (figure 5*e*,*f*). Consistent with the up-regulation of ALP gene expression, C3H10T1/2 cells cultured on surface-modified Ca–P/PHBV scaffolds loaded with rhBMP-2 also showed much higher OCN expression. It is well known that ALP and OCN are early and late osteogenic markers during osteogenic differentiation. These results indicated that the affinity of rhBMP-2 on immobilized heparin facilitated the osteogenic differentiation of C3H10T1/2 cells during the whole period of cell culture (21 days), probably because of to the sustained release of rhBMP-2 within this period. In the subsequent *in vivo* experiments, surface modified scaffolds loaded with rhBMP-2 were implanted into both muscle and ilium in a rabbit model. The results showed that the sintered nanocomposite scaffold with surface modification and rhBMP-2 improved bone regeneration after six-week implantation when compared with the scaffold without surface modification. In addition, ectopic osteogenesis was observed around surface-modified scaffold after 12-week implantation in muscle. Therefore, the nanocomposite scaffolds investigated in the current study could be potentially used to regenerate cortical bone and trabecular bone in non-load-bearing area or in load-bearing area but without the load-bearing function.

5. CONCLUSIONS

The current study shows that it is feasible to combine the SLS technique, nanocomposite material and sustained release of growth factor to form useful bone engineering scaffolds. It was demonstrated that scaffolds and porous structures of complex shape and architecture could be obtained through SLS. Based on various models, nanocomposite scaffolds or porous structure consisting of Ca–P nanoparticles and PHBV matrix were selectively sintered. The incorporation of Ca–P nanoparticles in scaffolds significantly improved SaOS-2 osteoblastic cell proliferation and ALP activity. The surface modification of Ca–P/PHBV nanocomposite scaffolds included gelatin entrapment and subsequent heparin immobilization. The surface modification improved the wettability of the scaffolds and provided binding affinity between conjugated heparin and growth factor rhBMP-2. The ALP activity of C3H10T1/2 MSCs on the surface-modified scaffolds loaded with rhBMP-2 was significantly higher than that of the cells on scaffolds with simple adsorption of rhBMP-2 during the 21-day osteogenic induction period. Furthermore, ALP and OCN osteogenic markers were upregulated for cells on surface modified scaffolds loaded with rhBMP-2, indicating the sustained release of rhBMP-2 during the 21 days. The creation of customized scaffolds with controlled architecture, osteoconductive nanocomposite and sustained release behaviour of osteogenic growth factor offers great potential for bone tissue engineering.

B.D. thanks the University of Hong Kong (HKU) for awarding him with the University Scholarship. This work was supported partly by a GRF grant (HKU 7176/08E) from the Hong Kong Research Grants Council and by a research grant from HKU. The authors thank Prof. Wai-Lam Cheung of HKU for his help in SLS, Dr Zhangyang Li and Prof. William W. Lu of HKU for their support in

conducting the cell culture work, and Prof. Changsheng Liu of East China University of Science and Technology for providing rhBMP-2.

REFERENCES

Ang, T. H., Sultana, F. S. A., Hutmacher, D. W., Wong, Y. S., Fuh, J. Y. H., Mo, X. M., Loh, H. T., Burdet, E. & Teoh, S. H. 2002 Fabrication of 3D chitosan-hydroxyapatite scaffolds using a robotic dispensing system. *Mater. Sci. Eng. C-Biomim. Supramol. Syst.* **20**, 35–42.

Berry, E., Brown, J. M., Connell, M., Craven, C. M., Efford, N. D., Radjenovic, A. & Smith, M. A. 1997 Preliminary experience with medical applications of rapid prototyping by selective laser sintering. *Med. Eng. Phys.* **19**, 90–96. (doi:10.1016/S1350-4533(96)00039-2)

Biondi, M., Ungaro, F., Quaglia, F. & Netti, P. A. 2008 Controlled drug delivery in tissue engineering. *Adv. Drug Deliv. Rev.* **60**, 229–242. (doi:10.1016/j.addr.2007.08.038)

Cai, K. Y., Yao, K. D., Yang, Z. M. & Li, X. Q. 2007 Surface modification of three-dimensional poly(D,L-lactic acid) scaffolds with baicalin: a histological study. *Acta Biomater.* **3**, 597–605. (doi:10.1016/j.actbio.2006.12.005)

Cao, Y., Croll, T. I., O'Connor, A. J., Stevens, G. W. & Cooper-White, J. J. 2006 Systematic selection of solvents for the fabrication of 3D combined macro- and microporous polymeric scaffolds for soft tissue engineering. *J. Biomater. Sci. Polym. Ed.* **17**, 369–402. (doi:10.1163/156856206776374142)

Capila, I. & Linhardt, R. J. 2002 Heparin–protein interactions. *Angew. Chemie-Int. Ed.* **41**, 391–412.

Chesnutt, B. M., Yuan, Y. L., Buddington, K., Haggard, W. O. & Bumgardner, J. D. 2009 Composite chitosan/nano-hydroxyapatite scaffolds induce osteocalcin production by osteoblasts *in vitro* and support bone formation *in vivo*. *Tissue Eng. Part A* **15**, 2571–2579. (doi:10.1089/ten.tea.2008.0054)

Chua, C. K., Leong, K. F., Cheah, C. M. & Chua, S. W. 2003*a* Development of a tissue engineering scaffold structure library for rapid prototyping. Part 1: investigation and classification. *Int. J. Adv. Manufact. Technol.* **21**, 291–301.

Chua, C. K., Leong, K. F., Cheah, C. M. & Chua, S. W. 2003*b* Development of a tissue engineering scaffold structure library for rapid prototyping. Part 2: parametric library and assembly program. *Int. J. Adv. Manufact. Technol.* **21**, 302–312.

Chung, H. J., Kim, H. K., Yoon, J. J. & Park, T. G. 2006 Heparin immobilized porous PLGA microspheres for angiogenic growth factor delivery. *Pharm. Res.* **23**, 1835–1841. (doi:10.1007/s11095-006-9039-9)

Duan, B. & Wang, M. 2008 Incorporation and release of biomolecules from Ca–P/PHBV nanocomposite tissue engineering scaffolds. In *Seventeenth Int. Symp. on Processing and Fabrication of Advanced Materials XVII*, pp. 881–891. New Delhi, India: I.K. International Publishing House Ltd.

Duan, B., Wang, M., Zhou, W. Y. & Cheung, W. L. 2008*a* Synthesis of Ca–P nanoparticles and fabrication of Ca–P/PHBV nanocomposite microspheres for bone tissue engineering applications. *Appl. Surf. Sci.* **255**, 529–533. (doi:10.1016/j.apsusc.2008.06.057)

Duan, B., Wang, M., Zhou, W. Y. & Cheung, W. L. 2008*b* Totally bioresorbable tissue engineering scaffolds based on Ca-P/PHBV nanocomposite and fabricated via selective laser sintering: Part III. Process optimization. *CD-ROM Proceedings of the 8th World Biomaterials Congress, Amsterdam, The Netherlands*, Paper #1309

Edlund, U., Danmark, S. & Albertsson, A. C. 2008 A strategy for the covalent functionalization of resorbable polymers with heparin and osteoinductive growth factor. *Biomacromolecules* **9**, 901–905. (doi:10.1021/bm701267u)

Fratzl, P., Gupta, H. S., Paschalis, E. P. & Roschger, P. 2004 Structure and mechanical quality of the collagen-mineral nano-composite in bone. *J. Mater. Chem.* **14**, 2115–2123. (doi:10.1039/b402005g)

Hart, G. W. 2009 *George W. Hart's Rapid Prototyping Web Page*. New York, NY: The State University of New York in Stony Brook. See http://www.georgehart.com/rp/rp.html. (accessed on 1st December 2009).

Heo, S. J. *et al.* 2009*a* *In vitro* and animal study of novel nano-hydroxyapatite/Poly(epsilon-caprolactone) composite scaffolds fabricated by layer manufacturing process. *Tissue Eng. Part A* **15**, 977–989. (doi:10.1089/ten.tea.2008.0190)

Heo, S. J., Kim, S. E., Wei, J., Hyun, Y. T., Yun, H. S., Kim, D. H., Shin, J. W. & Shin, J. W. 2009*b* Fabrication and characterization of novel nano- and micro-HA/PCL composite scaffolds using a modified rapid prototyping process. *J. Biomed. Mater. Res. Part A* **89A**, 108–116. (doi:10.1002/jbm.a.31726)

Ho, Y. C., Mi, F. L., Sung, H. W. & Kuo, P. L. 2009 Heparin-functionalized chitosan–alginate scaffolds for controlled release of growth factor. *Int. J. Pharm.* **376**, 69–75. (doi:10.1016/j.ijpharm.2009.04.048)

Hollister, S. J. 2009*a* Scaffold engineering: a bridge to where? *Biofabrication* **1**, 1–14. (doi:10.1088/1758-5082/1/1/012001)

Hollister, S. J. 2009*b* Scaffold design and manufacturing: from concept to clinic. *Adv. Mater.* **21**, 3330–3342. (doi:10.1002/adma.200802977)

Hutmacher, D. W., Sittinger, M. & Risbud, M. V. 2004 Scaffold-based tissue engineering: rationale for computer-aided design and solid free-form fabrication systems. *Trends Biotechnol.* **22**, 354–362. (doi:10.1016/j.tibtech.2004.05.006)

Jeon, O., Song, S. J., Kang, S. W., Putnam, A. J. & Kim, B. S. 2007 Enhancement of ectopic bone formation by bone morphogenetic protein-2 released from a heparin-conjugated poly(L-lactic-co-glycolic acid) scaffold. *Biomaterials* **28**, 2763–2771. (doi:10.1016/j.biomaterials.2007.02.023)

Jiao, X. Y., Billings, P. C., O'Connell, M. P., Kaplan, F. S., Shore, E. M. & Glaser, D. L. 2007 Heparan sulfate proteoglycans (HSPGs) modulate BMP2 osteogenic bioactivity in C2C12 cells. *J. Biol. Chem.* **282**, 1080–1086. (doi:10.1074/jbc.M513414200)

Karageorgiou, V. & Kaplan, D. 2005 Porosity of 3D biomaterial scaffolds and osteogenesis. *Biomateirals* **26**, 5474–5491. (doi:10.1016/j.biomaterials.2005.02.002)

Kim, J. Y. & Cho, D. W. 2009 The optimization of hybrid scaffold fabrication process in precision deposition system using design of experiments. *Microsyst. Technol. Micro Nanosyst. Info. Storage Process. Syst.* **15**, 843–851. (doi:10.1007/s00542-008-0727-8)

Kim, D., Yang, J. Y. & Shin, C. S. 2009 Overexpression of alpha-catenin increases osteoblastic differentiation in mouse mesenchymal C3H10T1/2 cells. *Biochem. Biophys. Res. Commun.* **382**, 745–750. (doi:10.1016/j.bbrc.2009.03.100)

Langer, R. & Vacanti, J. P. 1993 Tissue engineering. *Science* **260**, 920–926. (doi:10.1126/science.8493529)

Leong, K. F., Chua, C. K., Sudarmadji, N. & Yeong, W. Y. 2008 Engineering functionally graded tissue engineering scaffolds. *J. Mech. Behav. Biomed. Mater.* **1**, 140–152. (doi:10.1016/j.jmbbm.2007.11.002)

Li, J. J., Dou, Y., Yang, J., Yin, Y. J., Zhang, H., Yao, F. L., Wang, H. B. & Yao, K. D. 2009 Surface characterization and biocompatibility of micro- and nano-hydroxyapatite/chitosan-gelatin network films. *Mater. Sci. Eng. C Biomim. Supramol. Syst.* **29**, 1207–1215. (doi:10.1016/j.msec.2008.09.038)

Li, X., Koller, G., Huang, J., Di Silvio, L., Renton, T., Esat, M., Bonfield, W. & Edirisinghe, M. 2010 A novel jet-based nano-hydroxyapatite patterning technique for osteoblast guidance. *J. R. Soc. Interface* **7**, 189–197. (doi:10.1098/rsif.2009.0101)

Lin, R. Z. & Chang, H. Y. 2008 Recent advances in three-dimensional multicellular spheroid culture for biomedical research. *Biotechnol. J.* **3**, 1172–1184. (doi:10.1002/biot.200700228)

Lin, H., Zhao, Y., Sun, W. J., Chen, B., Zhang, J., Zhao, W. X., Xiao, Z. F. & Dai, J. W. 2008 The effect of crosslinking heparin to demineralized bone matrix on mechanical strength and specific binding to human bone morphogenetic protein-2. *Biomaterials* **29**, 1189–1197. (doi:10.1016/j.biomaterials.2007.11.032)

Liu, X. & Ma, P. 2009 Phase separation, pore structure, and properties of nanofibrous gelatin scaffolds. *Biomaterials* **30**, 4094–4103. (doi:10.1016/j.biomaterials.2009.04.024)

Liu, X. H., Won, Y. J. & Ma, P. X. 2005 Surface modification of interconnected porous scaffolds. *J. Biomed. Mater. Res. Part A* **74A**, 84–91. (doi:10.1002/jbm.a.30367)

Liu, L., Xiong, Z., Yan, Y. N., Hu, Y. Y., Zhang, R. J. & Wang, S. G. 2007 Porous morphology, porosity, mechanical properties of poly(alpha-hydroxy acid)-tricalcium phosphate composite scaffolds fabricated by low-temperature deposition. *J. Biomed. Mater. Res. Part A* **82A**, 618–629. (doi:10.1002/bjm.a.31177)

Lopez-Heredia, M. A., Sohier, J., Gaillard, C., Quillard, S., Dorget, M. & Layrolle, P. 2008 Rapid prototyped porous titanium coated with calcium phosphate as a scaffold for bone tissue engineering. *Biomaterials* **29**, 2608–2615. (doi:10.1016/j.biomaterials.2008.02.021)

Lv, Q., Nair, L. & Laurencin, C. T. 2009 Fabrication, characterization, and *in vitro* evaluation of poly(lactic acid glycolic acid)/nano-hydroxyapatite composite microsphere-based scaffolds for bone tissue engineering in rotating bioreactors. *J. Biomed. Mater. Res. Part A* **91A**, 679–691. (doi:10.1002/jbm.a.32302)

Lysaght, M. J., Jaklenec, A. & Deweerd, E. 2008 Great expectations: private sector activity in tissue engineering, regenerative medicine, and stem cell therapeutics. *Tissue Eng. Part A* **14**, 305–315. (doi:10.1089/tea.2007.0267)

Ma, X., Wu, X. M., Hu, Y. Y., Xiong, Z., Lv, R., Wang, J., Li, D. & Yan, Y. N. 2009 Intervertebral spinal fusion using a RP-based PLGA/TCP/bBMP biomimetic grafting material. *J. Bioact. Compat. Polym.* **24**, 146–157. (doi:10.1177/0883911509103830)

Mason, C. & Dunnill, P. 2009 Assessing the value of autologous and allogeneic cells for regenerative medicine. *Regen. Med.* **4**, 835–853. (doi:10.2217/RME.09.64)

Matsuda, N., Shimizu, T., Yamato, M. & Okano, T. 2007 Tissue engineering based on cell sheet technology. *Adv. Mater.* **19**, 3089–3099. (doi:10.1002/adma.200701978)

Melchels, F. P. W., Feijen, J. & Grijpma, D. W. 2009 A poly(D,L-lactide) resin for the preparation of tissue engineering scaffolds by stereolithography. *Biomaterials* **30**, 3801–3809. (doi:10.1016/j.biomaterials.2009.03.055)

Meng, D. C., Ioannou, J. & Boccaccini, A. R. 2009 Bioglass(A (R))-based scaffolds with carbon nanotube coating for bone tissue engineering. *J. Mater. Sci. Mater. Med.* **20**, 2139–2144. (doi:10.1007/s10856-009-3770-9)

Mironov, V., Visconti, R. P., Kasyanov, V., Forgacs, G., Drake, C. J. & Markwald, R. R. 2009 Organ printing: tissue spheroids as building blocks. *Biomaterials* **30**, 2164–2174. (doi:10.1016/j.biomaterials.2008.12.084)

Murugan, R. & Ramakrishna, S. 2005 Development of nanocomposites for bone grafting. *Compos. Sci. Technol.* **65**, 2385–2406. (doi:10.1016/j.compscitech.2005.07.022)

Naing, M. W., Chua, C. K., Leong, K. F. & Wang, Y. 2005 Fabrication of customised scaffolds using computer-aided design and rapid prototyping techniques. *Rapid Prototyping J.* **11**, 249–259. (doi:10.1108/13552540510612938)

Olivares, A. L., Marshal, E., Planell, J. A. & Lacroix, D. 2009 Finite element study of scaffold architecture design and culture conditions for tissue engineering. *Biomaterials* **30**, 6142–6149. (doi:10.1016/j.biomaterials.2009.07.041)

Peltola, S. M., Melchels, F. P. W., Grijpma, D. W. & Kellomaki, M. 2008 A review of rapid prototyping techniques for tissue engineering purposes. *Ann. Med.* **40**, 268–280. (doi:10.1080/07853890701881788)

Petzold, R., Zeilhofer, H. F. & Kalender, W. A. 1999 Rapid prototyping technology in medicine-basics and applications. *Comput. Med. Imaging Graph.* **23**, 277–284. (doi:10.1016/S0895-6111(99)00025-7)

Rohman, G., Baker, S. C., Southgate, J. & Cameron, N. R. 2009 Heparin functionalisation of porous PLGA scaffolds for controlled, biologically relevant delivery of growth factors for soft tissue engineering. *J. Mater. Chem.* **19**, 9265–9273. (doi:10.1039/b911625g)

Shea, C. M., Edgar, C. M., Einhorn, T. A. & Gerstenfeld, L. C. 2003 BMP treatment of C3H10T1/2 mesenchymal stem cells induces both chondrogenesis and osteogenesis. *J. Cell. Biochem.* **90**, 1112–1127. (doi:10.1002/jcb.10734)

Silva, N. A. *et al.* 2010 Development and characterization of a novel hybrid tissue engineering-based scaffold for spinal cord injury repair. *Tissue Eng. Part A* **16**, 45–54. (doi:10.1089/ten.tea.2008.0559)

Sokolsky-Papkov, M., Agashi, K., Olaye, A., Shakesheff, K. & Domb, A. J. 2007 Polymer carriers for drug delivery in tissue engineering. *Adv. Drug Deliv. Rev.* **59**, 187–206. (doi:10.1016/j.addr.2007.04.001)

Sundaray, B., Subramanian, V., Natarajan, T. S., Xiang, R. Z., Chang, C. C. & Fann, W. S. 2004 Electrospinning of continuous aligned polymer fibers. *Appl. Phys. Lett.* **84**, 1222–1224. (doi:10.1063/1.1647685)

Uebersax, L., Merkle, H. P. & Meinel, L. 2009 Biopolymer-based growth factor delivery for tissue repair: from natural concepts to engineered systems. *Tissue Eng. Part B Rev.* **15**, 263–289. (doi:10.1089/ten.teb.2008.0668)

Vasita, R. & Katti, D. S. 2006 Growth factor-delivery systems for tissue engineering: a materials perspective. *Expert Rev. Med. Devices* **3**, 29–47. (doi:10.1586/17434440.3.1.29)

Wang, E. A., Israel, D. I., Kelly, S. & Luxenberg, D. P. 1993 Bone morphogenetic protein-2 causes commitment and differentiation in C3H10T1/2 and 3T3 cells. *Growth Factors* **9**, 57–&71. (doi:10.3109/08977199308991582)

Wiria, F. E., Leong, K. F., Chua, C. K. & Liu, Y. 2007 Poly-epsilon-caprolactone/hydroxyapatite for tissue engineering scaffold fabrication via selective laser sintering. *Acta Biomater.* **3**, 1–12. (doi:10.1016/j.actbio.2006.07.008)

Wiria, F. E., Sudarmadji, N., Leong, K. F., Chua, C. K., Chng, E. W. & Chan, C. C. 2010 Selective laser sintering adaptation tools for cost effective fabrication of biomedical prototypes. *Rapid Prototyping J.* **16**, 90–99. (doi:10.1108/13552541011025816)

Woodfield, T. B. F., Guggenheim, M., von Rechenberg, B., Riesle, J., van Blitterswijk, C. A. & Wedler, V. 2009 Rapid prototyping of anatomically shaped,

tissue-engineered implants for restoring congruent articulating surfaces in small joints. *Cell Prolif.* **42**, 485–497. (doi:10.1111/j.1365-2184.2009.00608.x)

Xu, W., Wang, X. H., Yan, Y. N. & Zhang, R. J. 2008 Rapid prototyping of polyurethane for the creation of vascular systems. *J. Bioact. Compat. Polym.* **23**, 103–114. (doi:10.1177/0883911507088271)

Yang, P., Wang, C. S., Shi, Z. B., Huang, X., Dang, X. Q., Xu, S. L. & Wang, K. Z. 2009 Prefabrication of vascularized porous three-dimensional scaffold induced from rhVEGF(165): a preliminary study in rats. *Cells Tissues Organs* **189**, 327–337. (doi:10.1159/000142162)

Yeong, W. Y., Chua, C. K., Leong, K. F. & Chandrasekaran, M. 2004 Rapid prototyping in tissue engineering: challenges and potential. *Trends Biotechnol.* **22**, 643–652. (doi:10.1016/j.tibtech.2004.10.004)

Yoon, J. J., Chung, H. J., Lee, H. J. & Park, T. G. 2006 Heparin-immobilized biodegradable scaffolds for local and sustained release of angiogenic growth factor. *J. Biomed. Mater. Res. Part A* **79A**, 934–942. (doi:10.1002/jbm.a.30843)

Zhao, L., Li, G., Chan, K. M., Wang, Y. & Tang, P. F. 2009 Comparison of multipotent differentiation potentials of murine primary bone marrow stromal cells and mesenchymal stem cell line C3H10T1/2. *Calcif. Tissue Int.* **84**, 56–64. (doi:10.1007/s00223-008-9189-3)

Zhou, W. Y., Lee, S. H., Wang, M., Cheung, W. L. & Ip, W. Y. 2008 Selective laser sintering of porous tissue engineering scaffolds from poly(L)/carbonated hydroxyapatite nanocomposite microspheres. *J. Mater. Sci. Mater. Med.* **19**, 2535–2540. (doi:10.1007/s10856-007-3089-3)